Journal of Nuclear Materials 378 (2008) 35–39

Contents lists available at ScienceDirect

Journal of Nuclear Materials

journal homepage: www.elsevier.com/locate/jnucmat

Thermal conductivity mapping of pyrolytic carbon and silicon carbide coatings on simulated fuel particles by time-domain thermoreflectance

E. López-Honorato [a], C. Chiritescu [b], P. Xiao [a,*], David G. Cahill [b], G. Marsh [c], T.J. Abram [c]

[a] Materials Science Centre, School of Materials, The University of Manchester, Grosvenor Street, Manchester M1 7HS, UK
[b] Department of Materials Science and Engineering, Frederick Seitz Materials Research Laboratory, University of Illinois, Urbana, IL 61801, USA
[c] Nexia Solutions Ltd., Springfields PR4 0XJ, UK

ARTICLE INFO

Article history:
Received 17 February 2008
Accepted 18 April 2008

PACS:
81.15.Gh
78.20.Nv
65.60.+a
65.40.−b

ABSTRACT

Thermal conductivity of pyrolytic carbon and silicon carbide coatings on spherical particles has been mapped using time-domain thermoreflectance. The thermal conductivities measured for pyrolytic carbon ranged between 3.4 and 13.5 W/m K. The effect of porosity, pore-size distribution, anisotropy, in-plane disorder and domain sizes is discussed. A thermal conductivity of 168 W/m K was obtained for SiC. Mapping of the thermal conductivity of coated fuel particles provides useful data for modeling fuel performance during the operation of nuclear reactors.

1. Introduction

Renewed interest in nuclear energy around the world has engendered a renaissance of nuclear technology development in several countries. Two of the most promising technologies currently under study are the high temperature reactor (HTR) and very high temperature reactor (VHTR), generation III+ and generation IV nuclear reactors, respectively. Currently, both types of designs are based on a similar fuel unit called TRISO (tristructural isotropic) fuel particle. Three layers of pyrolytic carbon (PyC) and one of silicon carbide (SiC), or zirconium carbide, are placed on top of the fuel kernel in order to form a diffusion barrier and prevent the release of fission products [1]. The safety and efficiency of these reactor designs largely depends on the properties of these coatings, making their detailed characterization and fundamental understanding of their properties vitally important. However, despite the progress achieved in technology on HTR since the 1960s and 1970s when this idea was conceived, many of the characterization techniques for the TRISO particle currently being used remain almost the same as those used 30 years ago. Different groups have started to characterize these coatings with modern characterization techniques in order to provide more detailed information on these coatings and improve the knowledge on the fuel properties and performance, e.g. Raman spectroscopy, electron backscatter diffraction, nanoindentation and spectroscopic ellipsometry have already been used and have shown a great potential in replacing or complementing some of the old techniques [2–4].

Among the properties of PyC and SiC that are relevant to the nuclear industry, i.e., density, anisotropy of PyC and mechanical properties of SiC, thermal conductivity of the coatings has been one of the least studied. The key to nuclear power generation is to enable the heat generated to be transported to the coolant, i.e. helium gas, in the most efficient way. The knowledge of thermal conductivity of the fuel system not only enables the prediction of the thermal performance of the fuel but also to identify any possible temperature drop in the system, i.e. loss of efficiency. For example, if we consider the power generated by a fuel kernel to be around 0.25 W [5] (value that would vary depending on the content of uranium-235 and the position of the fuel within the reactor), and an as-produced thermal conductivity of 0.4 W/m K for a PyC layer with thickness of 100 μm (value previously measured for a buffer layer[6]) then the resulting temperature drop would be 57 K [7]. Furthermore, it is well known that during power generation fuel particles undergo several changes such as development of gaps at the interfaces, changes in grain structure, porosity, anisotropy, and O/U stoichiometry in UO_{2-x}. These changes not only have important effects on the mechanical properties of the coatings but also on their thermal conductivities, for example a gap formed between the buffer and IPyC resulting from dimensional changes produced by irradiation, could produce a further temperature drop of 55 K [5]. Additionally, because thermal conductivity affects the temperature of the fuel, and temperature controls the diffusion of fission products, the internal pressure of the particle and the

* Corresponding author. Tel.: +44 161 3065941; fax: +44 161 3063586.
E-mail address: Ping.xiao@manchester.ac.uk (P. Xiao).

0022-3115/$ - see front matter © 2008 Elsevier B.V. All rights reserved.
doi:10.1016/j.jnucmat.2008.04.007

stresses developed among coatings, which could cause the failure of the particle, it is crucial to study thermal conductivity of coated fuel particles.

Different studies have been carried out in the past in order to characterize the thermal properties of these fuel particles, however the majority have analyzed coatings deposited on rod or disk shaped substrates [8–12] instead of actual particles. The main concern on this method is that the coatings on a rod or disk shape substrate have different microstructure from those on spherical substrates [13,14]. Not until recently when Rochais et al. [6] characterized TRISO particles by photoreflectance microscopy has the thermal conductivity value for each layer been measured more accurately. The technique allows measurements of thermal conductivity of the individual PyC layers but not that of the SiC layer, due to its high thermal diffusivity. In this study we measured the thermal conductivity of the PyC and SiC layers of various fuel particles configurations using a thermal conductivity mapping method [15,16] based on the time-domain thermoreflectance technique (TDTR) [17,18]. Using this mapping method we are able to rapidly determine a cross-sectional profile of the thermal conductivity of various layers with large differences in thermal diffusivity such as PyC and SiC.

2. Experimental

2.1. Sample preparation

Three different samples were prepared using fluidized bed chemical vapor deposition [4,19,20]. Two single layer PyC coatings and a triple layered particle consisting of a buffer, inner pyrolytic carbon (IPyC) and silicon carbide (SiC) were deposited on alumina particles 500 μm in diameter. The single layer coatings were deposited with 50% v/v acetylene concentration at 1250 °C (1250-PyC) and 1450 °C (1450-PyC) (Figs. 2(a) and 3(a)). For the triple layered particle, a low density PyC (buffer) was produced with 40% v/v acetylene at 1450 °C, while the inner high density PyC (IPyC) was deposited with a mixture of 33% v/v acetylene/propylene at 1300 °C. The SiC layer was formed by the decomposition of methyltrichlorosilane (MTS) with a H_2/MTS = 277 at 1550 °C (Fig. 4(a)). Samples were embedded in epoxy resin and were ground with successive finer grades of SiC paper and polished up to a ¼ μm grit diamond paste and OPS solution. The density and texture (anisotropy) of the coatings produced are found in Table 1. Density was measured using the Archimedes method in ethanol. Texture was quantified by measuring the orientation angle obtained from azimuthal intensity scans of selected area electron diffraction (SAED) patterns from TEM samples (Fig. 1), using a similar method to that of Bourrat et al. [21]. A more detail description of the equipment and techniques used to prepare and characterize these samples can be found elsewhere [4].

2.2. Thermal conductivity measurements

Spot thermal conductivity measurements were performed on each layer of our samples using the TDTR method. A transducer layer of aluminum, 80–90 nm thick was deposited on the samples by RF magnetron sputtering prior to the thermal measurements. We split the output of a mode-locked Ti: sapphire laser (λ = 770 nm, 80 MHz repetition rate, <0.3 ps pulses) into a pump and probe beam. The pump beam was modulated using an electro-optic modulator (f = 9.8 MHz) and delayed with respect to the probe beam using a computer controlled mechanical stage. The pump and probe beams were focused at the sample surface using a single microscope objective lens with a 10 mm focal length, producing a $1/e^2$ radius of the focused spot w_0 = 3.1 μm. The total laser power at sample surface was 6 mW and created a steady-state temperature rise of up to 3 K in the alumina layer and ~1 K in the silicon carbide layer. The steady-state temperature rise in PyC layers was 16 K for sample 1250-PyC, 18 K for sample 1450-PyC, 5 K in the IPyC and 9 K in the buffer layer for the triple layered sample.

Table 1
Deposition conditions and general properties of the PyC and SiC coatings produced

Sample	Deposition conditions	Orientation angle (°)[a] (texture)	Coating thickness (μm)	Density (g/cm^3)[a]	Average thermal conductivity (W/m K)
1250-PyC	50%v/v Acy; 1250 °C	57 (medium texture)	29	2.12	4.2
1450-PyC	50% v/v Acy; 1450 °C	85 (low texture)	118	1.41	3.4
Buffer	40%v/v Acy; 1450 °C	–	71	1.35	5.7
IPyC	33% Acy/Prop; 1300 °C	43 (high texture)	30	2.0	13.5
SiC	H_2/MTS = 277; 1550 °C	–	13	–	168

Acy = acetylene; Prop = propylene; MTS = methyltrichlorosilane.
[a] Data taken from López-Honorato et al. [14].

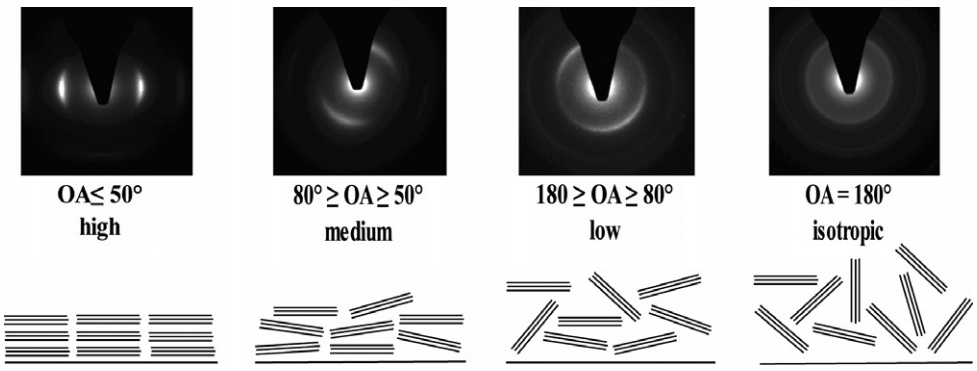

Fig. 1. Schematic representation showing the relationship between the preferred orientation of pyrolytic carbon domains (texture) and the orientation angle (OA) obtained from selected area electron diffraction (SAED) patterns.

The changes in the intensity of the reflected probe beam caused by the pump beam are recorded by a photodiode connected to a RF lock-in amplifier locked to the modulation frequency of the pump beam. The thermal conductivity of the sample is extracted by comparing the time dependence of the ratio Φ of the in-phase V_{in} and the out-of-phase V_{out} signals from the lock-in amplifier to calculations using a thermal diffusion model described in reference [18]. The model variables are the thermal conductivity Λ of the sample and the thermal conductance G of the Al/sample interface. The parameters of the model include the $1/e^2$ radius of the focused spot w_0, the thickness, heat capacity and thermal conductivity of the aluminum layer and the heat capacity of the sample (SiC, Al_2O_3 or PyC). The radius of the focused spot w_0 is determined from the dependence of V_{in} on the overlapping of the pump and probe beams. Aluminum film thickness was measured using picosecond acoustics [22,23]. Aluminum thermal conductivity was calculated using the Wiedemann–Franz law and 4-point probe measurements of the electrical resistivity. We used the literature values for heat capacities of Al [24] (2.4 J/cm^3 K at 300 K), SiC [25] (2.2 J/cm^3 K at 300 K) and Al_2O_3 [26] (3.1 J/cm^3 K at 300 K). The heat capacity of graphite [27,28] (1.6 J/cm^3 K at 300 K) was used as a basis for estimating the heat capacity of the pyrolitic carbon layers by multiplying the graphite heat capacity by the ratio of theoretical (2.26 g/cm^3) and reported (see Table 1) density of the sample.

We estimate the accuracy of the thermal conductivity measurement by calculating the square-root of the sum of the squares of uncertainties propagated from measurements of the fixed parameters of the model. The uncertainties propagated for each parameter are estimated by multiplying the experimental errors by the ratio of the sensitivity to the respective parameter and the sensitivity to the thermal conductivity of the sample. The sensitivity is defined as $S_\alpha = \mathrm{d}\ln\Phi/\mathrm{d}\ln\alpha$, where α is any parameter of the thermal model. The overall uncertainty in measuring the thermal conductivity of the sample layers is estimated at 10% for PyC and 5% in alumina and SiC.

For delay times in the range 100 ps < t < 500 ps, heat has diffused uniformly through the Al film but little heat has entered the sample because of the limited thermal conductance of the Al/sample interface (70–100 MW/m^2 K for our measurements). Thus, the in-phase thermoreflectance signal is proportional to $E/h_{Al}C_{Al}$, where $h_{Al}C_{Al}$ is the heat capacity per unit area of the Al film and E is the energy in each pump optical pulse. The out-of-phase thermoreflectance signal is proportional to the imaginary part of the frequency response at the modulation frequency of the pump beam. Since heat diffuses a distance in the sample that is large compared to the thickness of the Al film, the imaginary part of the frequency response is proportional to $P/(C\Lambda f)^{1/2}$, where $(C\Lambda)^{1/2}$ is the thermal effusivity of the sample, f is the modulation frequency of the pump beam, and P is the power of the pump beam. The ratio $V_{in}(t)/V_{out}(t)$ at short to intermediate delay times is therefore approximately proportional to $\Lambda^{1/2}$. We determined the thermal conductivity profiles by scanning the lateral cross-section of the sample at a fixed pump-probe delay time (115 ps) and recording the thermoreflectance signal V_{in}/V_{out} at each point. We use the thermal model and the parameters at one spatial location (usually a spot on the PyC layer) to calculate the range of thermal conductivities corresponding to a range of thermoreflectance ratios that encompasses the values we measured during scanning. The Λ vs. Φ curve is then fitted with a polynomial. We use the resulting function to convert the map of V_{in}/V_{out} ratios to a map of effective thermal conductivities $\Lambda_{eff.} = \Lambda C/C_0$. Λ and C are the thermal conductivity and heat capacity at each spatial location and C_0 is the heat capacity at the spatial location used for thermal profile conversion.

The scanning step size (pixel size) was 2 μm. The lateral resolution of the measurement is mostly controlled by the laser spot size. Because the thermoreflectance signal arises from the product of the pump and probe fluence, the effective spot size of the measurement is $w_0/\sqrt{2}$ (≈2 μm for w_0 = 3.1 μm).

3. Results

Figs. 2(b), 3(b) and 4(b) show the thermal conductivity maps and the line profiles of thermal conductivity across the coatings of the three samples which are shown in Figs. 2(a), 3(a) and 4(a). Interestingly the thermal conductivity images produced resemble those obtained by SEM, in which porosity as well as differences in density are clearly identified. Table 1 shows the thermal conductivities of the samples measured and their corresponding densities and orientation angles. The orientation angle measured based on the electron diffraction pattern represents the anisotropy of PyC [21] i.e. 180° indicates isotropic whereas a lower angle indicates more anisotropic [29] (Fig. 1). Average thermal conductivity values obtained from the thermal conductivity maps for PyC are 4.2

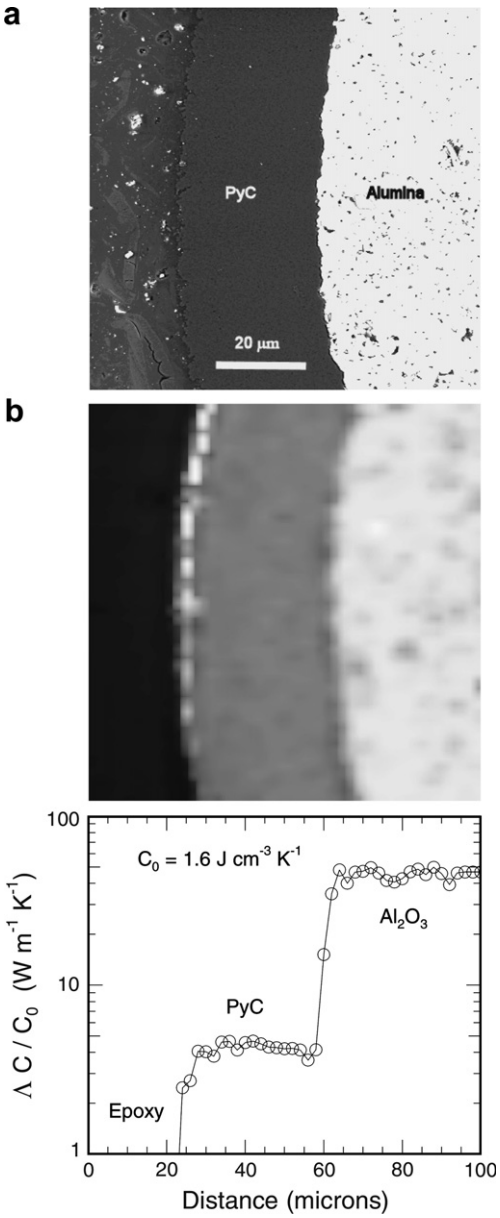

Fig. 2. Single layer high density coating produced at 1250 °C and 50% v/v acetylene concentration. (a) SEM image obtained for a similar sample; (b) thermal conductivity map. Individual layers are indicated in the line section plot. Error bars (not included) are 10% for the PyC layer and 5% for alumina.

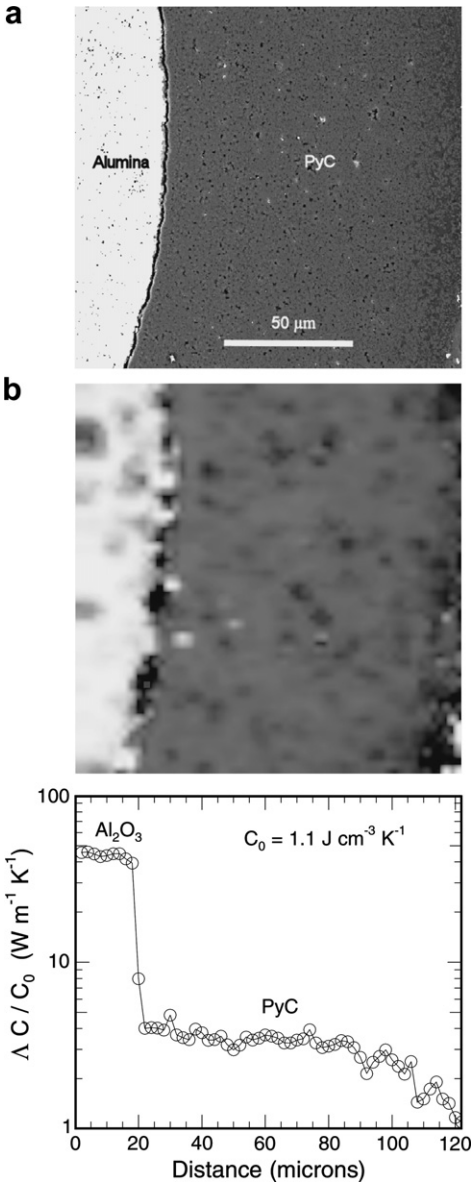

Fig. 3. Single layer low density coating produced at 1450 °C and 50% v/v acetylene concentration. (a) SEM image obtained for a similar sample; (b) thermal conductivity map. Error bars (not included) are 10% for the PyC layer and 5% for alumina.

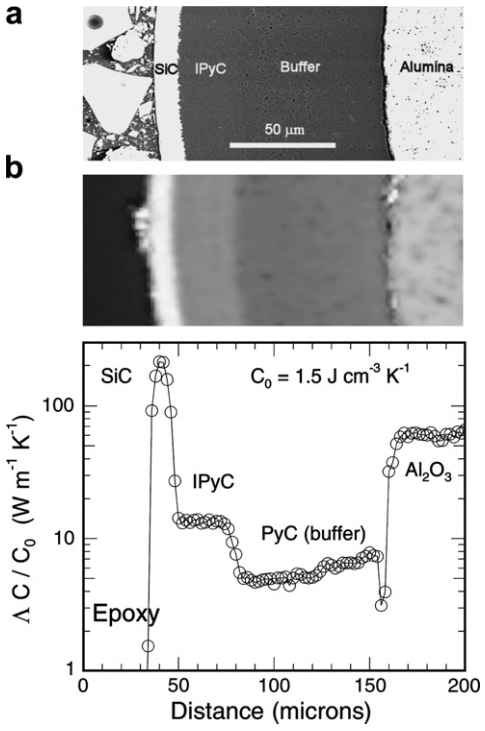

Fig. 4. Triple layer particle showing a buffer, IPyC and SiC layers. (a) SEM image obtained for similar sample; (b) thermal conductivity map. Individual layers are indicated in the line section plot. Error bars (not included) are 10% for the PyC layer and 5% for alumina and SiC.

W/m K for 1250-PyC and 3.4 W/m K for 1450-PyC with density values of 2.12 and 1.41 g/cm^3 respectively. For the triple layer coatings an average value of 5.7 W/m K and 13.5 W/m K were determined for the buffer PyC layer and inner PyC (IPyC) layers respectively, while the densities of the buffer and IPyC are 1.35 and 2 g/cm^3, respectively. It is important to mention that the deposition conditions used for the formation of the buffer layer were not the optimum conditions to obtain the standard density required for this layer of around 1 g/cm^3 [30]. For this reason the value of thermal conductivity quoted here should be higher than the value obtained for the PyC buffer layer in typical TRISO particles.

The values obtained in the present work are similar to the thermal conductivities measured in previous reports. Values between 0.7 and 11 W/m K have been reported [6,8,10,11,31] for PyC's with densities above 1.76 g/cm^3. On the other hand, thermal conductivities of around 0.2 W/m K have been measured for low density carbon (0.65 g/cm^3) and between 0.2 and 1.63 W/m K for different buffer layers [6,8,32].

The thermal conductivity measured for SiC (160 W/m K) was higher than the value reported by Salgado et al. [8] (16.74 W/m K) and Price [12] (62 and 50 W/m K). Nevertheless, if compared to high purity, defect free CVD SiC [33,34] with thermal conductivity of around 340 W/m K our value is much lower.

4. Discussion

The thermal conductivity in ceramic materials at room temperature is controlled by atomic vibrations (phonons) which can carry energy over lengths scales of a few angstroms to hundreds of nanometers depending on the structure of the material. In general it is accepted that higher amount of porosity (lower density) would result in lower thermal conductivities due to a decrease in the average atomic density and sound velocity. Although the effect of total porosity was confirmed for the two single layer PyC samples, in which lower thermal conductivity was measured for the low density material (1450-PyC), the changes in density alone do not explain all the differences observed among the samples. For example, the value obtained for the high porosity buffer layer (5.7 W/m K) was higher than that of both single layered-PyC's (3.4 and 4.2 W/m K), despite the fact that its density was lower (see Table 1). Furthermore, both high density PyC coatings (1250-PyC and IPyC) had a large difference in thermal conductivity (4.2 and 13.5 W/m K, respectively), even though the difference in density between them was very small. It is therefore evident than other factors also affect the thermal conductivity of PyC.

Rice [35] has mentioned that thermal conductivity is one of the properties that are controlled not only by the total amount of porosity but also by the type of porosity and its distribution. This idea has been corroborated by Ondracek and Schulz [36], who found that thermal conductivity on oxide nuclear fuel was mainly controlled by open porosity and specifically by pore sizes smaller

than 1 μm. Similarly Elbel and Vollath [37] found that different pore shapes, orientations and distributions would have different levels of influence on the thermal conductivity. The porosity distribution obtained by mercury immersion porosimetry showed that samples 1250- and 1450-PyC had larger amounts of open porosity below 100 nm than IPyC (33% v/v Acy/Prop) [14]. It is probable then that the large amount of open porosity below 100 nm would be partially responsible for the low thermal conductivity observed for the two single layer coatings.

Other differences between samples that could have affected thermal conductivity are anisotropy, domain size and structural disorder (inclusion of 5-member rings in the hexagonal structure). Smaller domain sizes and higher structural disorder might be able to produce phonon scattering, thereby reducing the phonon mean-free-path and decreasing thermal conductivity. The effect of anisotropy on thermal conductivity is controlled by the orientation of the graphene layers [31]. If higher anisotropic materials have graphene layers more parallel to the substrate surface, higher anisotropies would result in lower thermal conductivities in radial direction. Interestingly even thought IPyC had a considerable high anisotropy, the thermal conductivity (measured in the direction normal to the surface of the cross-section) of 1250-PyC was considerably different despite having slightly similar anisotropy.

The heat treatment suffered by both buffer and IPyC during the deposition of PyC and SiC could also have some effect on the microstructure and properties of PyC. Reznik et al. [38] have observed that heat treatment after PyC deposition might help in the dehydrogenation of the carbon material deposited, thus increasing its density and level of anisotropy. These effects could be also responsible for the difference in thermal conductivity between the IPyC and the outer PyC (OPyC) layers [6] where both layers although produced at similar deposition conditions would experience different heat treatments.

For the SiC layer, the differences between the value measured in this work and that reported previously might come from differences in the stoichiometry of SiC and their crystallite sizes. For example, the SiC measured by Price [12] was deposited at 1400 °C, a temperature at which Si is usually codeposited with SiC if no other reactant is included (i.e. Ar or C_3H_6) in addition of MTS and H_2. High thermal conductivity SiC could be obtained by increasing its purity (reducing excess Si or C and avoiding α-SiC), lowering defect concentration, and increasing crystal size (not desirable since larger crystal sizes would allow the diffusion of fission products). All these characteristics would lead to minimization of phonon scattering. For our particular case, excess Si or C is not the reason for the intermediate thermal conductivity measured since Raman spectroscopy of the SiC show the presence of only β-SiC, as consequence the reduction in thermal conductivity was probably due to phonon scattering produced by crystal size boundaries or internal defects. Current development of SiC coatings on TRISO particles is to produce SiC with nanometric scale equiaxed grains sizes in order to reduce the diffusion of fission products and improve the mechanical properties of the SiC, whereas these changes may lead to change in thermal conductivity of SiC. In addition, radiation damage seriously decrease thermal conductivity due to the formation of simple defects and defect-clusters (point defect regime) [39]. Therefore the combined effect of nanometric scale grains together with radiation damage will have to be studied if an accurate understanding of the TRISO fuel particle is desired.

5. Conclusions

Due to combination of high spatial resolution and capability to produce a thermal conductivity map over a 200 by 200 μm area, time-domain thermoreflectance has proved to be a valuable tool in determination of thermal conductivity of coated particles. The thermal conductivity map shows small variations across the coating layers and indicates uniformity of the coatings. Thermal conductivities between 3.4 and 13.5 W/m K were measured for PyC coatings with different densities and microstructures. The changes in total porosity alone did not explain the observed differences. Porosity, together with anisotropy, structural disorder and domain size appear to affect the thermal conductivity of PyC. SiC conductivity of 168 W/m K was obtained.

Acknowledgements

The authors gratefully acknowledge the valuable assistance of X. Zhao and P.J. Meadows. The authors would also like to thank Nexia Solutions Ltd. for the financial support provided and CONACYT-México for a PhD Grant to E. López-Honorato. C.C. and D.G.C. acknowledge support from DOE BES, Division of Materials Sciences under Award No. DEFG02-91ER45439, through Materials Research Laboratory at the University of Illinois at Urbana-Champaign. Thermal conductivity measurements were performed in the Laser and Spectroscopy Facility at Frederick Seitz Materials Research Laboratory, University of Illinois, which is partially supported by the US Department of Energy under Grant DEFG02-91-ER45439.

References

[1] G.H. Lohnert, H. Nabielek, W. Schenk, Nucl. Eng. Des. 109 (1988) 257.
[2] G.E. Jellison Jr., J.D. Hunn, R.A. Lowden, J. Nucl. Mater. 352 (2006) 6.
[3] D. Helary, O. Dugne, X. Bourrat, P.H. Jouneau, F. Cellier, J. Nucl. Mater. 350 (2006) 332.
[4] E. López-Honorato, P.J. Meadows, P. Xiao, G. Marsh, T.J. Abram, Nucl. Eng. Des. (2008), 10.1016/j.nucengdes.2007.11.022.
[5] D.G. Martin, Nucl. Eng. Des. 213 (2002) 241.
[6] D. Rochais, G. Le Meur, G. Domingues, V. Basini, in: Proceedings of the Third International Topical Meeting on High Temperature Reactor Technology, Johannesburg, South Africa, October 2006.
[7] F.P. Incropera, D.P. de Wit, Fundamentals of Heat and Mass Transfer, 4th Ed.., John Wiley, New York, 1996.
[8] P.G. Salgado, F.P. Schilling, G.T. Brock, K.L. Holman, Nucl. Technol. 11 (1971) 131.
[9] D.W. Stevens, Nucl. Appl. 3 (1967) 626.
[10] J.C. Bokros, R.J. Price, K. Koyama, Carbon 4 (1966) 293.
[11] K.E. Gilchrist, High Temp. High Press. 4 (1972) 497.
[12] R.J. Price, J. Nucl. Mater. 46 (1973) 268.
[13] G. Hofmann, M. Wiedenmeier, M. Freund, A. Beavan, J. Hay, G.M. Pharr, Carbon 38 (2000) 545.
[14] E. López-Honorato, P.J. Meadows, P. Xiao, Carbon (submitted for publication).
[15] S. Huxtable, D.G. Cahill, V. Fauconnier, J.O. White, J–C Zhao, Nat. Mater. 3 (2004) 298.
[16] X. Zheng, D.G. Cahill, J.-C. Zhao, Adv. Eng. Mater. 7 (2005) 622.
[17] C.A. Paddock, G.L. Eesley, J. Appl. Phys. 60 (1986) 285.
[18] D.G. Cahill, Rev. Sci. Instrum. 75 (2004) 5119.
[19] C. Vahlas, F. Juarez, R. Feurer, P. Serp, B. Caussat, Chem. Vapor Depos. 8 (2002) 127.
[20] R.L.R. Lefevre, M.S.T. Price, Nucl. Technol. 35 (1977) 263.
[21] X. Bourrat, B. Trouvat, G. Limousin, G. Vignoles, J. Mater. Res. 15 (2000) 92.
[22] H.T. Grahn, H.J. Maris, J. Tauc, IEEE J. Quantum Electron. 25 (1989) 2562.
[23] K.E. O'Hara, X. Hu, D.G. Cahill, J. Appl. Phys. 90 (2001) 4852.
[24] D.A. Ditmars, C.A. Plint, R.C. Shukla, Int. J. Thermophys. 6 (1985) 499.
[25] K.K. Kelley, J. Am. Chem. Soc. 63 (1941) 1137.
[26] D.C. Ginnings, G.T. Furukawa, J. Am. Chem. Soc. 75 (1953) 522.
[27] W. DeSorbo, W.W. Tyler, J. Chem. Phys. 21 (1953) 1660.
[28] A.T.D. Butland, R.J. Maddison, J. Nucl. Mater. 49 (1973) 45.
[29] B. Reznik, K.J. Hüttinger, Carbon 40 (2002) 621.
[30] H. Huschka, P. Vygen, Nucl. Technol. 35 (1977) 238.
[31] G.A. Slack, Phys. Rev. 127 (1962) 694.
[32] R. Taylor, High Temp. High Press. 4 (1972) 649.
[33] J. Li, L. Porter, S. Yip, J. Nucl. Mater. 255 (1998) 139.
[34] L.L. Snead, J. Nucl. Mater. 329–333 (2004) 524.
[35] R.W. Rice, Porosity of Ceramics, Marcel Dekker, New York, 1998.
[36] G. Ondracek, B. Schulz, J. Nucl. Mater. 46 (1973) 253.
[37] H. Elbel, D. Vollath, J. Nucl. Mater. 153 (1988) 50.
[38] B.R. Reznik, K. Norinaga, D. Gerthsen, O. Deutschman, Carbon 44 (2006) 1330.
[39] L.L. Snead, T. Nozawa, Y. Katoh, T-S. Byun, S. Kondo, D.A. Petti, J. Nucl. Mater. 371 (2007) 329.